10

Effect of Buoyancy on Pore-Scale Characteristics of Two-Phase Flow in Porous Media

Tetsuya Suekane and Hiroki Ushita
The University of Tokushima
Japan

1. Introduction

Carbon dioxide (CO_2) is the most important anthropogenic greenhouse gas. The global atmospheric concentration of CO_2 has increased from a pre-industrial value of approximately 280 ppm to 379 ppm in 2005. The warming of the climate system is unequivocal, as is now evident from observations of increasing global average air and ocean temperatures, widespread melting of snow and ice and rising global average sea level (IPCC, 2007a). To stabilize the concentration of CO_2 in the atmosphere, emissions need to peak and then decline thereafter. In the long term, energy conservation, efficiency improvements in energy conversion, lower carbon fuels such as natural gas and renewable energy sources are the most promising alternatives. For lower stabilization targets, scenarios put more emphasis on the use of low-carbon energy sources, such as renewable energy and nuclear power, and the use of CO_2 capture and storage (CCS; Pacala & Socolow, 2004; IPCC, 2007b); however, the transition from the current dependence on fossil fuels would take many decades. The capture of CO_2 from fossil fuel power plants and other large-scale stationary emission sources and storage in geologic formations is the only option that permits a transition from current high-intensity carbon-based energy sources to low-carbon energy sources.

The safety of geologic storage of CO_2 is obviously a central concern in planning carbon sequestration on a large scale. The current concept of geologic storage involves the injection of CO_2 into deep formations, which typically contain brine. CO_2 is supercritical at temperatures and pressures above the critical values of 304 K and 7.38 MPa. In typical geologic formations, the critical condition of CO_2 is reached at a depth of approximately 740 m. Because of geologic pressure, the density of CO_2 dramatically increases with depth; however, the density of CO_2 is approximately 0.9 times that of water, so when CO_2 is injected into the subsurface, buoyancy tends to bring CO_2 upward in geologic formations. On the other hand, CO_2 will be retained by physical and geochemical mechanisms, such as physical trapping (IPCC 2005), capillary trapping (Suekane et al. 2008, 2010a; Al Mansoori et al. 2010; Pentland et al. 2010; Zhou et al. 2010; Wildenschild et al. 2010; Saadatpoor 2010), solubility trapping (Lindeberg & Wessel-Berg 1997; McPherson & Cole 2000; Ennis-King et al. 2003; Gilfillan et al. 2009; Iding & Blunt 2010) and mineralization (Gunter et al. 1993).

Capillary trapping is sometimes referred to as residual gas trapping or relative permeability hysteresis trapping. When CO_2 is injected into the subsurface, it spreads in geologic formations in a continuous phase, displacing brine. As it migrates through a formation, the saturation of CO_2 decreases and some of it is retained in pore space by capillary forces. In the case of Berea sandstone, residual CO_2 saturation ranges from 24.8 to 28.2% at supercritical conditions (Suekane et al. 2008). Once the gas bubbles are trapped, they are stable against water flow, because the capillary forces acting on the gas bubbles are much higher than buoyancy and viscous sheer stress (Suekane et al. 2010a; Zhou et al. 2010).

Saturation of CO_2 trapped by capillarity also depends on numerous factors, such as how the wetting fluid gets in (either by forced or spontaneous imbibition), the rate of imbibition, CO_2 saturation at flow reversal and the properties of porous media (Holtz 2002; Suekane et al. 2010b). In the case of the Sleipner project, CO_2 was injected into a point approximately 200 m below the caprock. The CO_2 plume spreads upward by buoyancy before accumulating below the caprock (IPCC 2005; Arts et al. 2008). On the other hand, in the case of oil production by gas-assisted gravity drainage (GAGD) processes, crestal gas injection uses wells in higher structural positions close to the top of the reservoir. GAGD has been considered to be a very attractive oil recovery process because of its higher efficiency (Hagoort 1980; de Mello et al. 2009; Rostami et al. 2010). When gas is injected vertically downward into the formations, the higher sweep efficiency could be achieved with the aid of stabilization of a displacement front by buoyancy. For upward displacement of fluids by buoyant gas, however, fingering and instability of a displacement front reduces the sweep efficiency and gas saturation. The gas saturation at the flow reversal has strong influence on the residual gas saturation.

In this study, the effect of the stability of a displacing front in gravity drainage on the initial gas saturation is discussed using dimensionless parameters and the relationship between initial gas saturation and residual gas saturation is explored. Gas injection experiments were carried out with packed beds of glass beads using a nitrogen and water system in laboratory conditions. The three-dimensional structure of the distribution of gas in the packed beds was visualized by means of a microfocused X-ray CT scanner. Water was injected into the packed beds to evaluate the residual gas saturation. Finally, gas was injected vertically upward into the packed bed to study the effect of the direction of gas injection with respect to gravity on the gas saturation.

2. Experiments

2.1 Experimental apparatus and procedure

Glass beads with a diameter of 100 µm, 200 µm or 400 µm were packed in an acrylic resin tube with an interior diameter of 10 mm and a height of 40 mm (Fig. 1a). First, the packed bed was soaked in water. After gas contained in the packed bed was evacuated by a vacuum pump, water was forced into pore spaces during the recovery of ambient pressure to atmospheric pressure. Next the packed bed, aligned vertically, was connected by Teflon tube to a gas reservoir containing nitrogen at a pressure of 0.12 MPa and a syringe pump filled with water (Fig. 1b). Nitrogen was injected into the packed bed vertically downward or upward at a constant flow rate, by withdrawing water into the syringe pump at a constant flow rate. Five units of pore volume (PV) of nitrogen were injected into the packed bed. This condition is often referred to as an irreducible water condition, where the remaining water in a porous media is immobile. In this paper, we define the gas saturation at this condition to be the initial gas saturation. Then, the packed bed was disconnected from the tubing systems and placed in an X-ray CT scanner

(Comscantechno Co. ScanXmate-RB090SS) to observe the distribution of gas and water. Following the CT scan, the packed bed was connected again to the syringe pump (Fig. 1c). Five PV of water was injected vertically upwards into the packed bed at a constant flow rate. The resulting condition is referred to as the residual gas condition, where gas bubbles are trapped by capillarity in porous media. The saturation at this condition is referred as residual gas saturation. The packed bed was scanned by the X-ray CT scanner again. An X-ray CT scan was performed at the steady state of the packed bed after each gas or water injection.

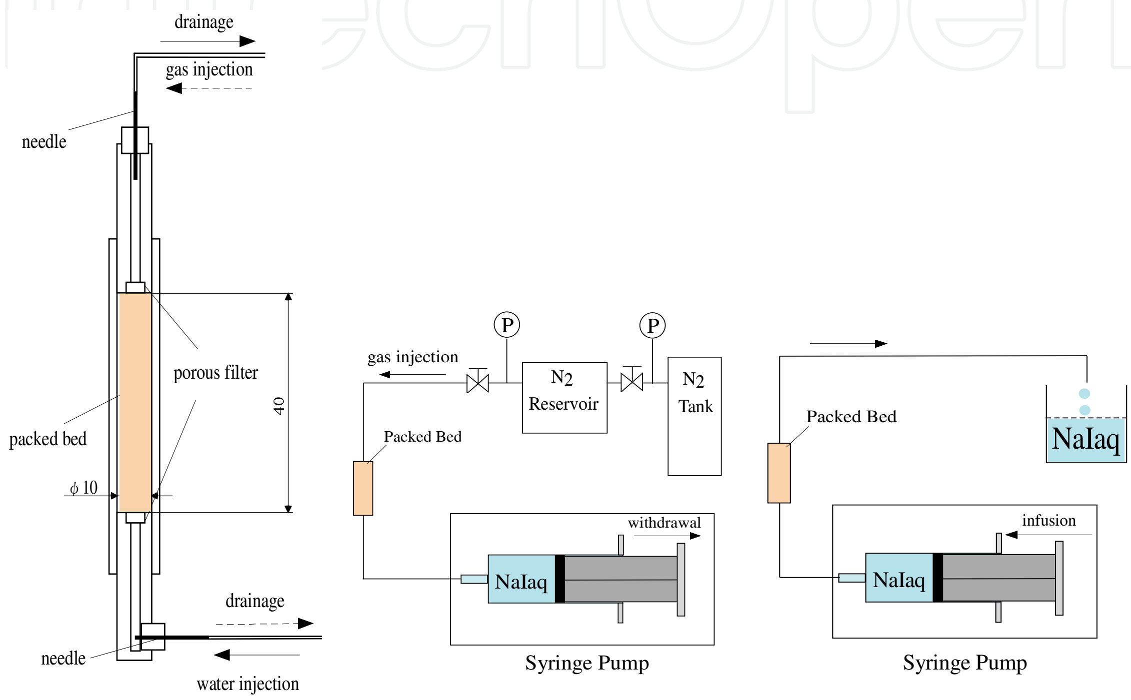

Fig. 1. Schematic views of (a) the packed bed of glass beads, (b) experimental setup for the drainage process and (c) experimental setup for the imbibition process.

2.2 Dimensionless parameters and experimental conditions
2.2.1 Dimensionless parameters
Two-phase flows in porous media are influenced by interfacial tension, buoyancy and viscous sheer stress. The Bond number (Bo) and capillary number (Ca) are defined as

$$Bo = \frac{(\rho_w - \rho_n) g R^2}{\sigma} \tag{1}$$

$$Ca = \frac{\mu_w v}{\sigma}, \tag{2}$$

where ρ is the density, g is the acceleration due to gravity, R is the particle radius, σ is interfacial tension, μ is the viscosity, v is the displacing fluid velocity and subscripts w and n denote the wetting phase and non-wetting phase, respectively. Bo and Ca represent the ratio of buoyancy force and of viscous sheer stress to the capillary force, respectively. Instead of

Equation 1, the Dombrowski–Brownell number, which is the ratio of the pore scale hydrostatic pressure drop to the capillary pressure (Rostami et al. 2010), is defined as

$$N_{DB} = \frac{(\rho_w - \rho_n) g (k/\phi)}{\sigma}, \tag{3}$$

where k is the absolute permeability and ϕ is the porosity. The semi-heuristic Carman-Kozney model of permeability predicts the permeability of packed beds as follows (Kaviany 1995):

$$k = \frac{\phi^3}{45(1-\phi)^2} R^2 . \tag{4}$$

For gravity drainage processes, which correspond to vertically downward injections of gas into the packed bed in the current experiments, the critical gravity drainage velocity is defined by Blackwell and Terry (1959) and Dumore (1964) as

$$v_c = \frac{(\rho_w - \rho_n) g k}{\mu_w} . \tag{5}$$

The critical gravity drainage velocity depends on the difference in the density, the viscosity of drained fluid and the permeability of porous media. In the current experiments, because we used the nitrogen and water system in laboratory conditions, the critical gravity drainage velocity depends only on the radius of glass beads from equation 5. The ratio of the critical gravity drainage velocity to the displacing fluid velocity, vc/v, is referred to as the stability parameter.

2.2.2 Experimental conditions

All experiments were performed for the nitrogen and water system in laboratory conditions. The fluid properties of the nitrogen and water system and the supercritical CO_2 and water system at a typical reservoir condition, which corresponds to the depth of approximately 850 m, are summarized in Table 1.

		Viscosity, μ (μPa·s)	density, ρ (kg/m^3)	interfacial tension, σ (mN/m)	Ca	Bo
Reservoir condition (318 K, 8.5 MPa)	sc CO_2	20	259.6	35.7	$1.681 \times 10^{-2} \times v$	$2.017 \times 10^{5} \times R^2$
	H_2O	600	993.9			
Laboratory condition (293 K, 0.1 MPa)	gas N_2	17.87	1.123	72.6	$1.463 \times 10^{-2} \times v$	$1.345 \times 10^{5} \times R^2$
	H_2O	1062	996.7			

Table 1. Fluid properties under experimental conditions and typical reservoir conditions.

We used nitrogen as a non-wetting phase instead of CO_2 for these experiments to reduce the dissolution in water. Interfacial tension between supercritical CO_2 and water is approximately half of that between nitrogen and water in laboratory conditions. Because of the high density of supercritical CO_2 with respect to nitrogen, buoyancy is also lower for supercritical CO_2. As a result, the Bond number falls in a similar range.

The water used in the experiments was doped with sodium iodide (NaI) at 7.5 wt% to enhance the X-ray attenuation. Henceforth, for simplicity, this aqueous phase is referred to as water. During drainage processes, the injection flow rate of nitrogen was controlled by a syringe pump to cause the capillary number to be in the range between 3.72×10^{-7} and 1.86×10^{-5}. Depending on the radius of the glass beads, the stability parameter vc/v ranges from 0.05 to 37.9. In imbibition processes, the injection flow rate of water was controlled such that the capillary number was 1.00×10^{-6}.

Reconstructed three-dimensional images are 608 × 608 × 610 pixels at a resolution of 25.048 μm/pixel in all directions.

3. Results and discussion

3.1 Stability effect of gravity drainage on gas saturation

3.1.1 Stable gravity drainage

Nitrogen was injected vertically downward into the packed bed filled with water at various flow rates to investigate the effect of the instability of a displacing front on gas saturation. Figure 2 shows vertical cross-sectional images around the axis of the packed bed. For drainage at stability parameters of 9.2 and 1.8, high initial gas saturations, Sg*, of 91 and 85%, respectively, are achieved without the effect of gas fingering with the aid of a stable interface of displacement. When the displacement velocity is above the critical gravity drainage velocity, large fractions of water remain in the packed bed. At stability parameters lower than 0.36, fingering of injected gas results in gas saturations below 25%. The distribution of gas shown in Fig. 2 suggests that the critical gravity drainage velocity defined by equation 5 gives an appropriate criterion for the stability of a drainage interface.

3.1.2 Fingering

Figure 3 shows vertical cross-sectional images after the unstable drainage of vc/v = 0.36 for four independent experimental runs under the same conditions, where the capillary number is 9.30×10^{-6} and the Bond number is 5.38×10^{-3}. Because the drainage is unstable, fingering has a great influence on gas distributions. Reflecting the nature of instability, the initial gas saturation varies widely from 22 to 67%. Because the glass beads on the surface of cylindrical tube tend to be sorted, the porosity at the region adjacent to the surface is higher than that at the centre of the packed bed. Figure 3c suggests that heterogeneity in porosity enhances the effect of fingering and reduces the displacement efficiency.

3.1.3 Effect of capillary number on initial gas saturation

The effect of capillary number on the initial gas saturation is shown in Fig. 4 for packed beds of glass beads with the diameters 100 μm, 200 μm and 400 μm. With an increase in capillary number, the initial gas saturation decreases, as has been reported by many researchers (Morrow & Songkran, 1982; Chatzis et al. 1983; Morrow et al. 1988; Rostami et al. 2010). At a capillary number of 9.30×10^{-6} with 200-μm diameter glass beads, the initial gas saturation varies widely due to fingering of the interface (Fig. 3). At a low capillary number of 3.72×10^{-7}, an initial gas saturation of more than 70% can be achieved, even for the fine glass beads.

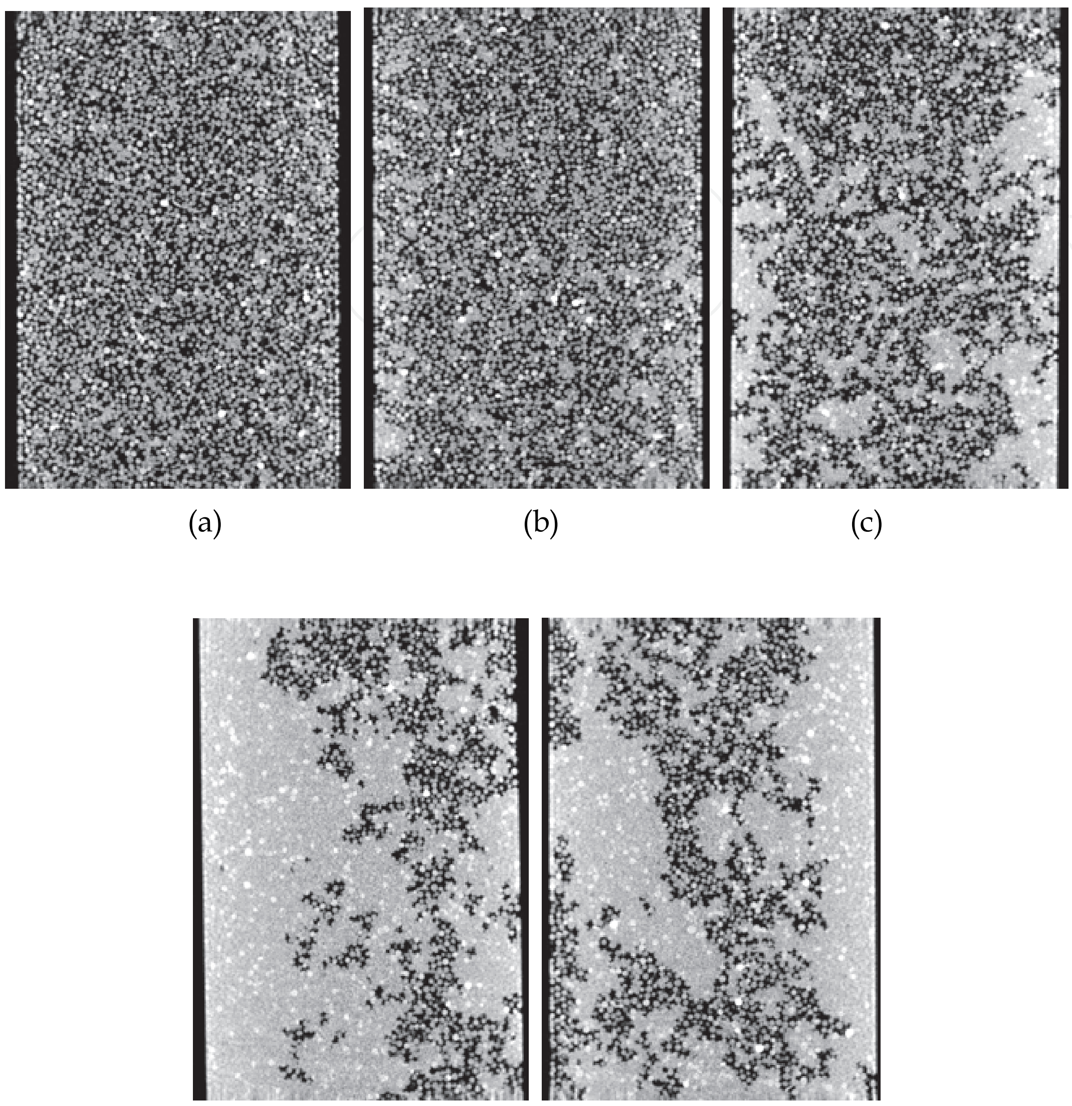
(a) (b) (c)
(d) (e)

Fig. 2. Effect of the stability parameter vc/v on gravity drainage by gas injection. (a) Ca = 1.86×10^{-7}, vc/v = 9.2, Sg* = 91% (b) Ca = 3.72×10^{-7}, vc/v = 1.8, Sg* = 85% (c) Ca = 1.86×10^{-6}, vc/v = 0.92, Sg* = 69% (d) Ca = 9.30×10^{-6}, vc/v = 0.36, Sg* = 25% (e) Ca = 1.86×10^{-5}, vc/v = 0.18, Sg* = 24%. Glass beads with a diameter of 200 μm were packed in a tube with an inner diameter of 10 mm, shown as black regions at the image edge.

3.1.4 Bond number effect on initial gas saturation

The effect of Bond number on the initial gas saturation is shown in Fig. 5 for packed beds of glass beads with various diameters at a constant injection flow rate corresponding to a capillary number of 3.72×10^{-7}. Because the higher Bond number results in a more stabilized displacement front, higher displacement efficiency could be achieved for high Bond numbers (Fig. 4).

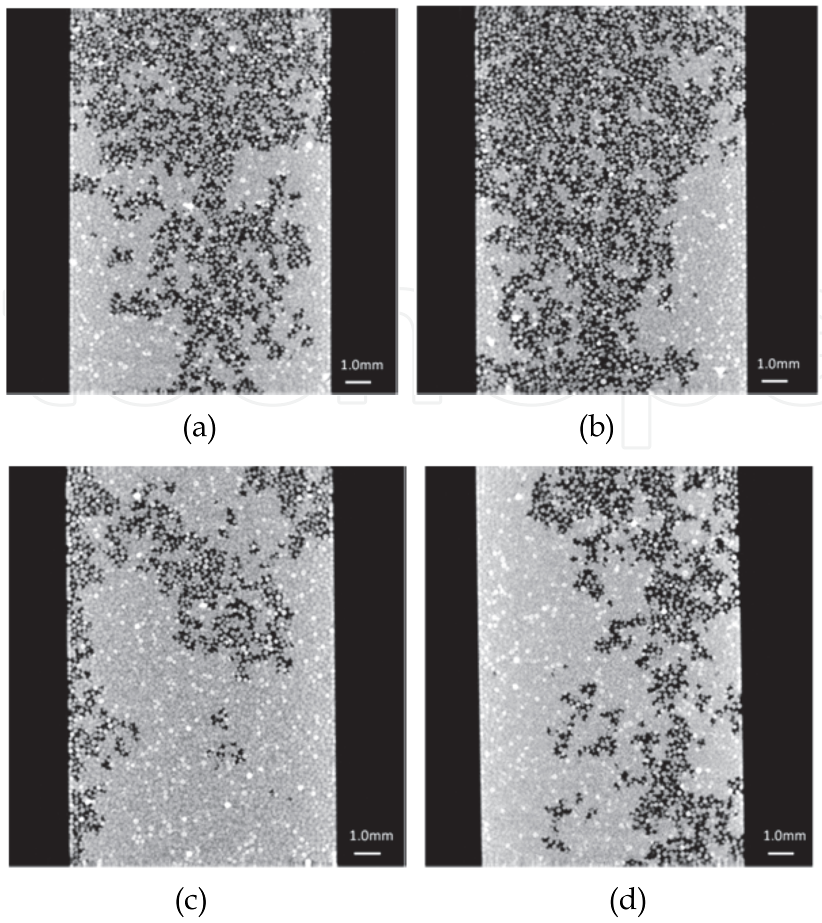

Fig. 3. Reproducibility of gravity drainage in the unstable condition where Ca = 9.30×10^{-6} and Bo = 5.38×10^{-3}.

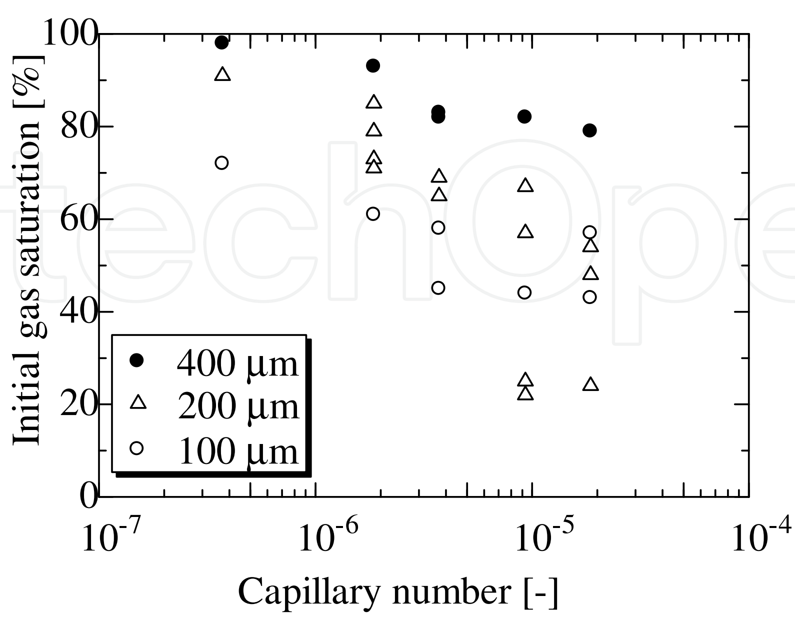

Fig. 4. Effect of capillary number on the initial gas saturation for drainage processes with downward gas injection.

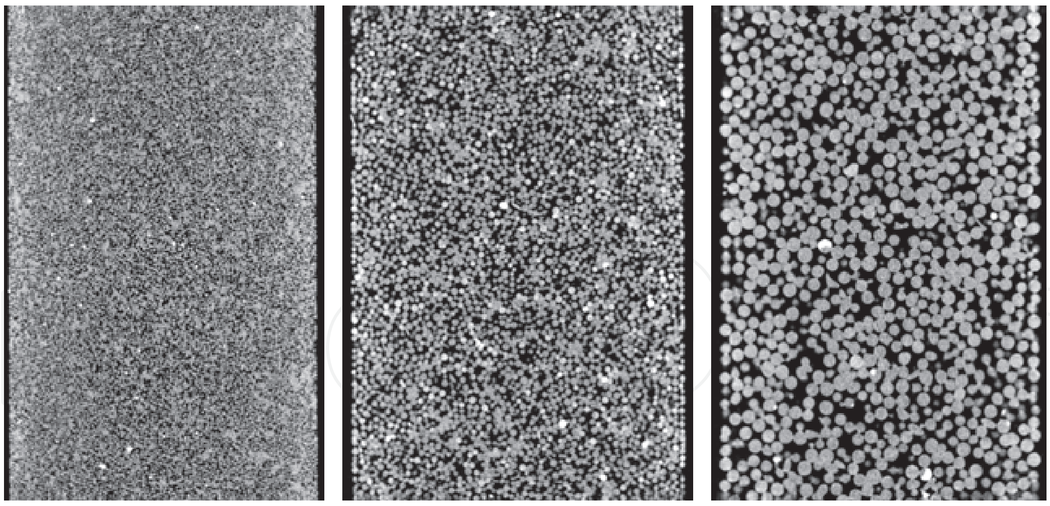

Fig. 5. Bond number effect on gravity drainage by gas injection at the capillary number of 3.72×10^{-7}. (a) Bo = 3.36×10^{-4}, R = 50 μm (b) Bo = 1.35×10^{-3}, R = 100 μm (c) Bo = 5.38×10^{-3}, R = 200 μm.

The Bond number effect on the initial gas saturation for drainage processes is shown in Fig. 6 for various capillary numbers. With an increase in Bond number, the initial gas saturation increases. With higher diameter glass beads, the higher critical gravity drainage velocity results in the higher displacement efficiency associated with the reduction in capillary force (Rostami et al. 2010). The displacement front of drainage is stable for all experimental runs shown in Fig. 5. Therefore, for the large, 400 μm glass beads, an extremely high gas saturation of 98% can be achieved at a high Bond number. This is an attractive fact that suggests high oil recovery of GAGD.

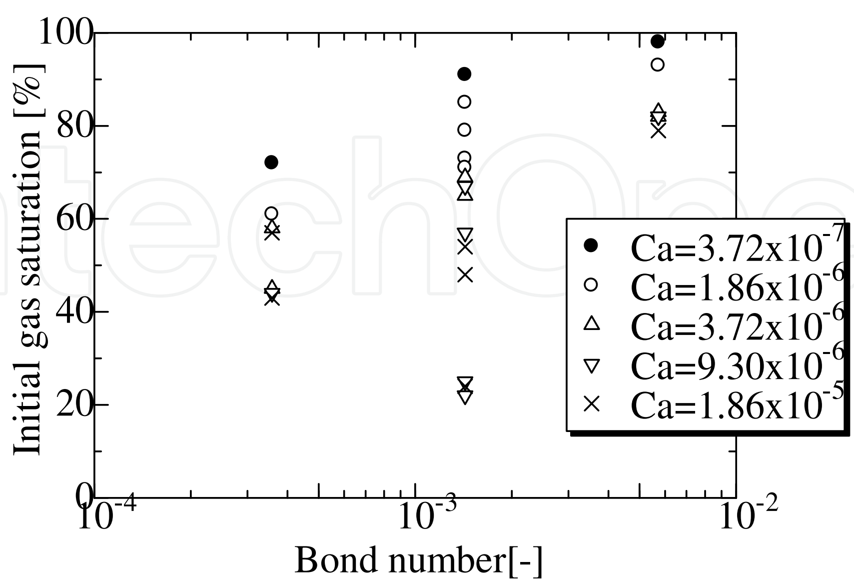

Fig. 6. Bond number effect on the initial gas saturation for drainage processes with downward injection of gas.

3.2 Effect of initial gas saturation on residual gas saturation

3.2.1 Morphology of trapped gas bubbles

Water is injected vertically upward into the packed bed of glass beads at a constant flow rate, which corresponds to a capillary number of 1.0×10^{-6}, after gravity drainage processes. Figure 7 shows the distributions of gas after drainage processes and the distributions of trapped gas bubbles after the imbibition processes for each diameter of glass beads. Because of low gas-injection flow rate at a capillary number of 3.72×10^{-7}, high initial gas saturations are achieved for each packed bed after the drainage processes (Fig. 7a–c). Into these packed beds, 5 PV of water was injected vertically upwards at a capillary number of 1.0×10^{-6}. Distributions of trapped gas bubbles are shown in Fig. 7d–f for each diameter of glass beads. As the diameter of glass beads decreases, residual gas saturation increases because the capillary force becomes high compared with buoyancy. Gas is perfectly non-wetting to glass beads. Therefore, gas bubbles with low volume are trapped at the centre of pore spaces. Gas bubbles with a volumetric scale of several pores are trapped in the packed beds spreading over several pores without surface contact of glass beads by thin water films.

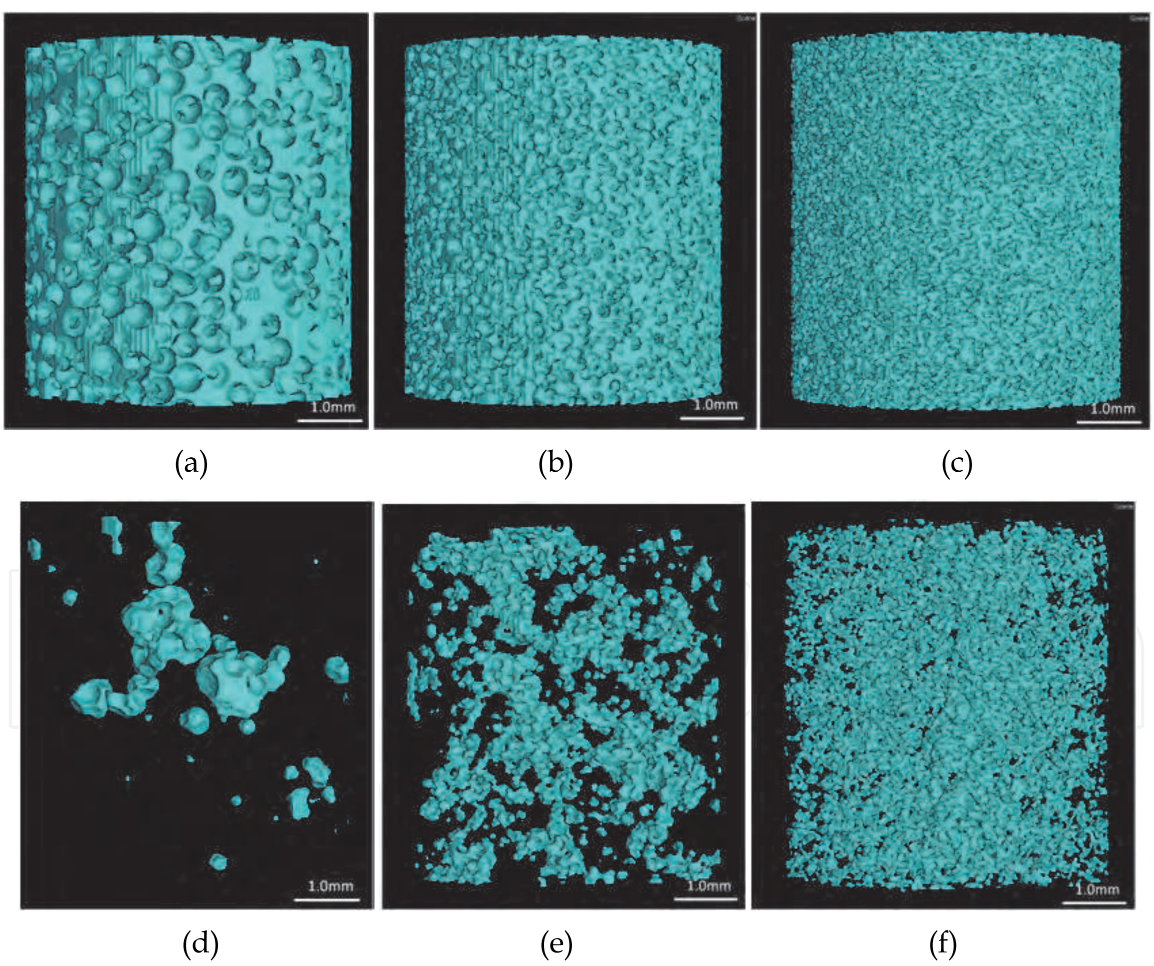

Fig. 7. Distributions of injected gas after stable drainage (a–c) and trapped gas bubbles after water imbibition (d–e) for the packed bed of glass beads with a diameter of (a, d) 400 µm, (b, e) 200 µm and (c, f) 100 µm. Surface of the gas in the cylindrical domain with a diameter of 5 mm and a length of 5 mm is visualized.

Distributions of the volume of trapped gas bubbles are shown in Fig. 8. The volume of gas bubbles were analysed using the image processing software ImageJ (Abramoff et al. 2004; Rasband 1997–2008) with some plug-ins for the cylindrical domain at a diameter of 9 mm and length of 2.5 mm. The volume of bubbles is normalized with that of packed glass beads. For lower diameter glass beads, the largest gas bubble tends to be large compared to the glass bead. The volume of the largest bubble in the packed bed of 400 μm glass beads is approximately one order of magnitude larger than that of the glass bead. On the other hand, in a packed bed of 100 μm glass beads, the volume of the largest bubble is approximately 73,000 times as large as that of a glass bead. This largest gas bubble contains approximately 98% of all trapped gas.

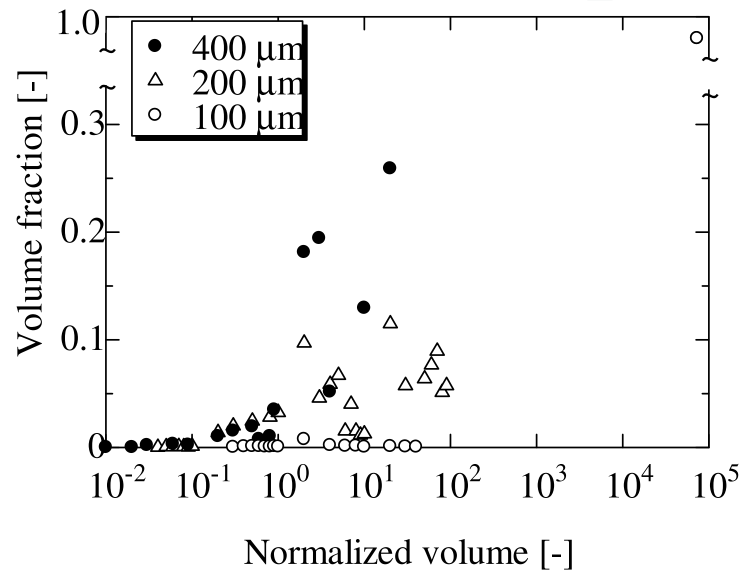

Fig. 8. Distribution of the volume of trapped gas bubbles in packed beds of glass beads with various diameters. The volume of gas bubbles is normalized with that of a glass bead in the packed bed. Vertical axis denotes the volume fraction with respect to the total volume of trapped gas.

3.2.2 Relationship between initial and residual gas saturations

An increase in the injection flow rate of gas results in a decrease in the initial gas saturation (Fig. 4) because of the instability of displacing fronts. Residual gas saturation is affected by initial gas saturation, even for water injection at the same capillary number. The relationship between the initial gas saturation and residual gas saturation is shown in Fig. 9. The residual gas saturation peaks against the initial gas saturation at approximately 50%. An inverse trend between initial gas saturation and residual gas saturation has been found in unconsolidated sandstone (Holtz 2002) and in the packed bed (Suekane et al. 2010b). During imbibition processes, the migration of gas is assisted by buoyancy, because water is injected vertically upward. For higher initial gas saturations, gas in a continuous phase is hardly disconnected from the continuum. Because the displacing front of water is stabilized by buoyancy, the branch of gas jutting from the continuum into water retreats due to buoyancy before being disconnected by capillary forces (Setiawan et al. 2010). From a viewpoint of the safety of geologic storage of CO_2, the difference between initial and residual gas saturations, which denotes the fraction of CO_2 escaping through a porous media, would be reduced by the design of injection strategy to adjust the initial gas saturation.

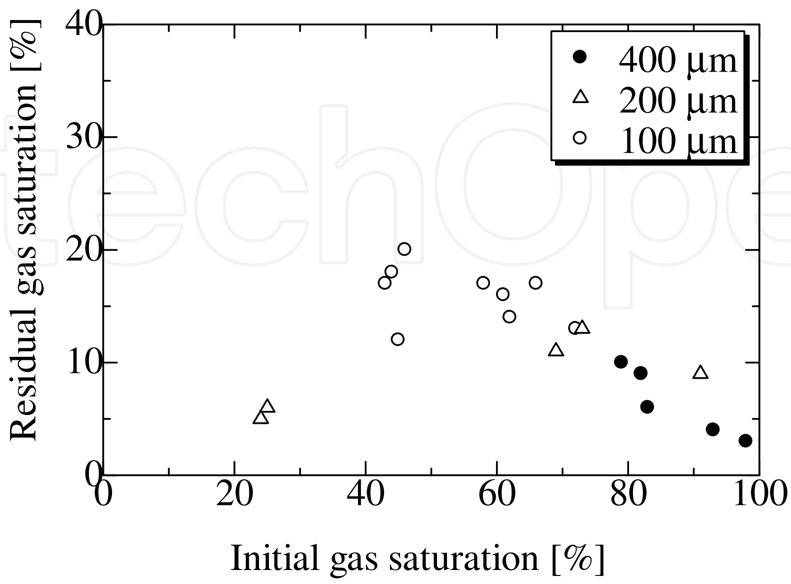

Fig. 9. Relationship between the initial and residual gas saturations.

3.2.3 Stability of gravity drainage and gas trapping

The initial gas saturation for the packed bed of 400 μm glass beads after drainage at stability parameters vc/v of 37.9 and 0.76, was 98 (Fig. 7a) and 79%, respectively. After water imbibition, the residual gas saturation was 3 and 10%, respectively, and the trapped gas bubbles are shown in Figs. 7d and 10, respectively. Distribution of the volume of trapped gas bubbles is shown in Fig. 11. In the case of unstable drainage, even though the initial gas saturation is lower than that in the case of stable drainage, residual gas saturation is high, because large bubbles with the scale of several pore sizes remain in porous media.

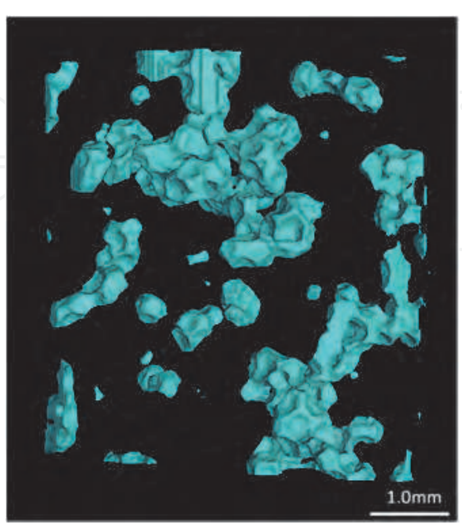

Fig. 10. Trapped gas bubbles in the packed bed of 400 μm glass beads at a residual gas saturation of 10%, after unstable drainage at a stability parameter vc/v of 0.76.

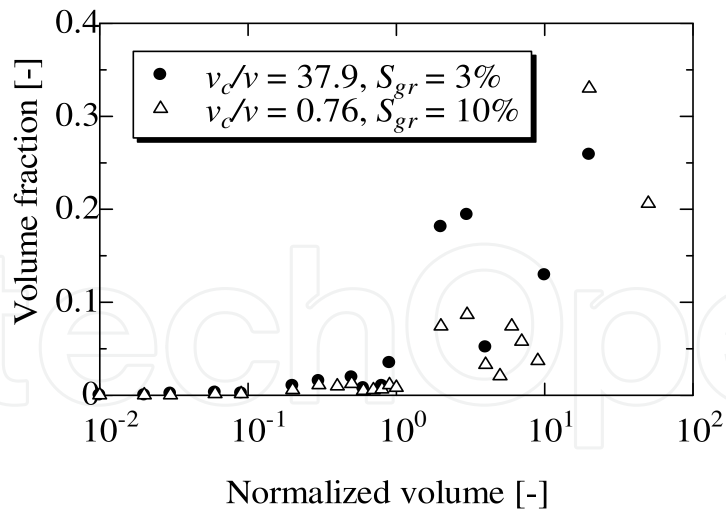

Fig. 11. Distribution of the volume of trapped gas bubbles in packed beds of 400 μm glass beads. After drainage at stability parameters vc/v of 37.9 and 0.76, water was injected at a capillary number of 1.0×10^{-6}. The volume of gas bubbles is normalized with that of a glass bead in the packed bed.

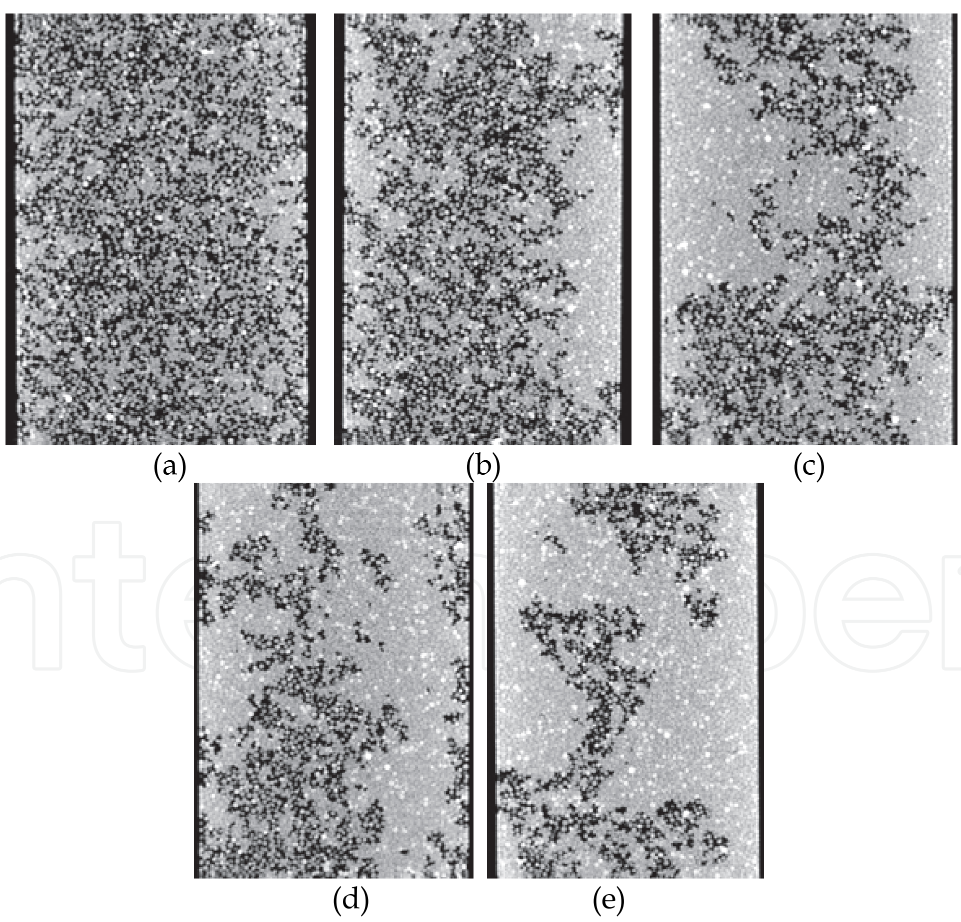

Fig. 12. Vertically upward drainage by gas injection at a capillary number of (a) Ca = 1.86×10^{-7}, (b) Ca = 3.72×10^{-7}, (c) Ca = 1.86×10^{-6}, (d) Ca = 9.30×10^{-6}, (e) Ca = 1.86×10^{-5}. Glass beads with a diameter of 200 μm were packed in tube with an inner diameter of 10 mm, shown as black regions at the image edges.

3.3 Upward drainage

In this section, we injected gas vertically upward as is often the case in actual CCS projects. The packed bed of glass beads and experimental setup used in the experiments were the same as that shown in Fig. 1, except for the direction of gas injection.

Figure 12 shows vertical cross-sectional images at various injection flow rates of gas. Except for the direction of gas injection, gas injection flow rates in Fig. 12a–e are the same as those in Fig. 2a–e, respectively. The initial gas saturations are compared for the direction of gas injection in Fig. 13. In the case of the upward injection of gas, gravitational force and capillary pressure let water remain in porous media against gas migration. With a decrease in the gas injection flow rate, the initial gas saturation increases; however, the initial gas saturation at the upward gas injection is lower than that at the downward gas injection at the same capillary number because of instability of displacing front.

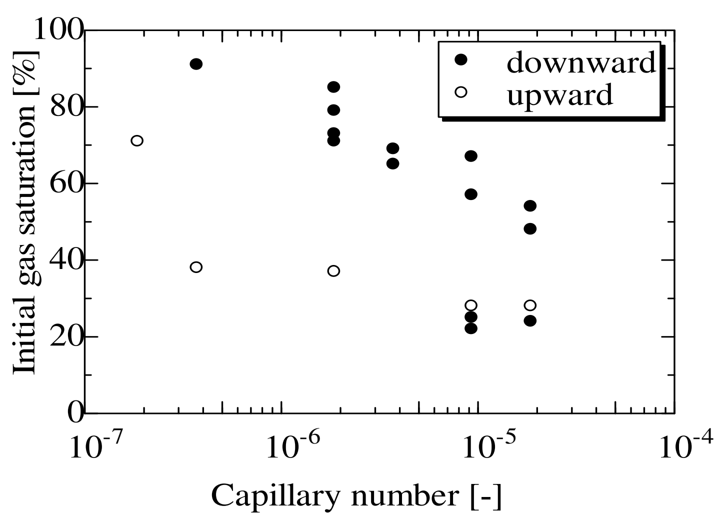

Fig. 13. Effect of the direction of gas injection on the initial gas saturation at various capillary numbers.

4. Conclusion

Gas injection experiments were carried out using packed beds of glass beads with a nitrogen and water system in laboratory conditions. The three-dimensional structure of the distribution of gas in the packed beds was visualized by means of a microfocused X-ray CT scanner.

First, the effect of the stability of a displacing front in gravity drainage on the initial gas saturation was discussed with dimensionless parameters. For gravity drainage in stable conditions, high initial gas saturation is achieved without the effect of gas fingering with the aid of a stable interface of displacement. When the displacement velocity is above the critical gravity drainage velocity, large fractions of water remain in the packed bed. Reflecting the nature of instability, the initial gas saturation varies widely from drainage to drainage. Heterogeneity in porosity enhances the effect of fingering and reduces the displacement efficiency. With an increase in Bond number and a decrease in capillary number, the initial gas saturation increases. In the packed bed of 400μm glass beads, an extremely high gas saturation of 98% can be achieved at a capillary number of 3.72×10^{-7}.

Next, water was injected in the packed beds to evaluate the residual gas saturation. The residual gas saturation has a peak against the initial gas saturation at approximately 50%.

During imbibition processes, migration of gas is assisted by buoyancy because water is injected vertically upward. For higher initial gas saturations, gas in a continuous phase is hardly disconnected from the continuum.

Finally, gas was injected vertically upward into the packed bed to study the effect of the direction of gas injection with respect to gravity on gas saturation. In the case of the upward injection of gas, gravitational forces and capillary pressure let water remain in porous media against gas migration. With a decrease in the gas injection flow rate, the initial gas saturation increases; however, the initial gas saturation due to upward gas injection is lower than that due to downward gas injection at the same capillary number because of instability of the displacing front.

5. References

Abramoff, M. D.; Magelhaes, P. J. & Ram, S. J. (2004). Image processing with image. *J. Biophotonics Int.*, Vol. 11, pp. 36-44

Al Mansoori, S.K.; Itsekiri, E.; Iglauer, S.; Pentland, C.H.; Bijeljic, B. & Blunt, M.J. (2010). Measurements of Non-Wetting Phase Trapping Applied to Carbon Dioxide Storage. *International Journal of Greenhouse Gas Control*, Vol. 4, pp. 283-288

Arts, R.; Chadwick, A.; Eiken, O.; Thibeau, S. & Nooner, S. (2008). Ten Year's Experience of Monitoring CO_2 Injection in the Utsira Sand at Sleipner, Offshore Norway. first break, Vol. 26, (January 2008) pp. 66-72

Blackwell, J.T. & Terry, M.W. (1959). Factors Influencing the Efficiency of Miscible Displacement. Transactions of AIME. Vol. 216, pp. 1-8

Chatzis, I.; Morrow, N.R. & Lim, H.T. (1983). Magnitude and Detailed Structure of Resiual Oil Saturation. Society of Petroleum Engineers Journal, (April 1983), pp. 311-326

de Mello, S.F.; Trevisan, O.V. & Schiozer D.J. (2009) Review on Gravity Dreainage Performance, Presented at 20th International Congress of Mechanical Engineering, Grambado, RS, Brazil, November 15-20, 2009

Dumore, J.M. (1964). Stability Consideration in Downward Miscible Displacement. Society of Petroleum Engineers Journal. Vol. 4, pp. 356-362

Ennis-King, J; Gibson-Poole, C.M.; Lang, S.C. & Paterson, L. (2003). Long Term Numerical Simulation of Geological Storage of CO_2 in the Petral Sub-Basin, North West Autralia. Proceeding of 6th Internationl Conference on Greenhouse Gas Control Technologies, J. Gale & Y. Kaya (eds.) Vol. 1, Kyoto, Japan, Octover 1-4, 2002

Gilfillan, S.M.V.; Lollar, B.S.; Holland, G.; Blagburn, D.; Stevens, S.; Schoell, M.; Cassidy, M.; Ding, Z.; Zhou, Z.; Lacrampre-Couloume, G. & Ballentine, C.J. (2009). Solubility Trapping in Foramtion Water as Dominant CO_2 Sink in Natural Gas Fields. Nature, Vol. 458, (April 2009), pp. 614-618

Gunter, W.D.; Perkins, E.H. & McCann, T.J. (1993). Aquifer Dsposal of CO_2-Rich Gases: Reaction Design for Added Capacity. Energy Conversion and Management. Vol. 34, pp. 941-748

Hagoort, J. (1980) Oil Recovery by Gravity Drainage. Society of Petroleum Engineers Journal. (June 1980) pp. 139-150

Holtz, M.H. (2002). Residual Gas Saturation io Aquifer Influx: A Calculation Method for 3-D Computer Reservoir Contruction. Presented at the SPE Gas Technology Symposium, Alberta, Canada, April 30–May 2, 2002 SPE 75502

Iding, M. & Blunt, M.J. (2010) Enhanced Solubility Trapping of CO_2 in Fractured Resrvoirs, Presented at 10th International Conference on Greenhouse Gas Control Technologies, Amsterdam, The Netherlands, September 19-23, 2010

IPCC, (2005). IPCC Special Report on Carbon Dioxide Capture and Storage. Metz, B.; Davidson, O.; de Coninck, H.C.; Loos, M. & Meyer, L.A. (eds.), Cambridge University Press, Cambridge, UK and USA pp. 195-276

IPCC, (2007a). Climate Change 2007: The Physical Science Basis. Contribution of waroking Group I to the Frouth Assessment Report of the Intergovernmental Panel on Climate Change. S. Solomon; D. Qin; M. Manning; Z. Chen; M. Marquis; K.B. Averyt; M. Tignor & H.L. MIller (eds.), Chambridge University Press, ISBN 978-0-521-70597-7 New York, USA

IPCC, (2007b). Climate Change 2007: Mitigation of Climate Change. Contribution of waroking Group III to the Frouth Assessment Report of the Intergovernmental Panel on Climate Change. B. Metz; O.R. Davidson; P.R. Bosch; R. Dave & L.A. Meyer (eds.), Chambridge University Press, ISBN 978-0-521-70598-1 New York, USA

Kaviany, M. (1995). Principles of Heat Transfer in Porous Media. Springer-Verlag New York, Inc., ISBN 0-387-94550-4, New York, USA

Lindeberg, E. & Wessel-Berg, D. (1997). Vertical Convection in an Aquifer Column under a Gas Cap of CO_2. Energy Conversion and Management. Vol. 38 No. Suppl. pp. S229-S234

McPherson, B.J.O.J. & Cole, B.S. (2000). Multiphase CO_2 Flow, Transport and Sequestration in the Powder River Basin, Wyoming, USA. Journal of Geochemical Exploration, Vol. 69-70, No.6, pp. 65-70

Morrow, N.R. & Songkran, B. (1982). Effect of Viscous and Buoyancy Forces on Nonwetting Phase Trapping in Porous Media, In: Surface Phenomena in Enhanced Oil Recovery, D.O. Shah (ed.), 287-411, Plenum Press, New York City

Morrow, N.R.; Chatzis, I. & Taber, J.J. (1988). Entrapment and Mobilization of Residual Oil in Bead Packs. SPE Reservoir Engineering, (August 1988), pp. 927-934

Pacala, S. & Socolow, R. (2004). Stabilization Wedge: Solving the Climate Problem for the Next 50 Years with Current Technolgies. Science, Vol. 305, No. 5686, (August 2004), pp. 968-972

Pentland C.H.; El-Maghraby, R.; Georgiadis, A.; Iglauer, S. & Blunt, M.J. (2010) Immiscible Displacement and Capillary Trapping in CO_2 Storage. Presented at 10th International Conference on Greenhouse Gas Control Technologies, Amsterdam, The Netherlands, September 19-23, 2010

Rasband, W. S. (1997-2008) ImageJ [Internet]. Bethesda (Maryland, USA): US National Institute of Health. Available from: http://rsbweb.nih.gov/ij/.

Rostami, B.; Kharrat, R.; Pooladi-Darvish, M. & Ghotbi, C. (2010). Identification of Fluid Dynamics in Forced Gravity Drainage Using Dimensionless Goups. Trasport in Porous Media, Vol. 83, pp. 725-740

Saadatpoor, E., Bryant, S.L. & Sepehrnoori, K. (2010). Effect of Upscaling Heterogeneous Domain on CO_2 Trapping Mechanisms. Presented at 10th International Conference on Greenhouse Gas Control Technologies, Amsterdam, The Netherlands, September 19-23, 2010

Setiawan, A.; Nomura, H. & Suekane, T. (2010). Pore-scale visualization of imbibition process in porous media by using X-ray CT scanner, *presented at 7th International Conference of Flow Dynamics*, Sendai, Japan, November 1-3, 2010
Suekane, T.; Nobuso, T.; Hirai, S. & Kiyota, M. (2008) Geological Storage of Carbon Dioxide by Residual Gas and Solubility Trapping. International Journal of Greenhouse Gas Control, Vol. 2, No.1, pp. 58-64
Suekane, T.; Zhou, N.; Hosokawa, T. & Matsumoto, T. (2010a) Direct Observation of Gas Bubbles Trapped in Sandy Porous Media. Transport in Porous Media, Vol. 82, No. 1, pp. 111-122
Suekane, T.; Zhou, N. & Hosokawa, T. (2010b) Maximization of Capillary Trapping Ratio to Injected CO_2 by Means of Co-injection. Presented at 10th International Conference on Greenhouse Gas Control Technologies, Amsterdam, The Netherlands, September 19-23, 2010
Wildenschild, D.; Armstrong R.T.; Herring, A.L.; Young, I.M. & Carey, J.W. (2010) Exploring Capillary Trapping Efficiency as a Function of Interfacial Tension, Viscosity, and Flow Rate. Presented at 10th International Conference on Greenhouse Gas Control Technologies, Amsterdam, The Netherlands, September 19-23, 2010
Zhou, N.; Matsumoto, T.; Hosokawa, T. & Suekane, T. (2010) Pore-Scale Visualization of Gas Trapping in Porous Media by X-ray CT Scanning. Flow Measurement and Instrumentation, Vol. 21, pp. 262-267

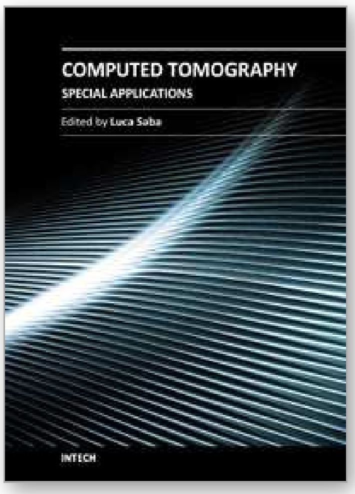

ISBN 978-953-307-723-9
Hard cover, 318 pages
Publisher InTech
Published online 21, November, 2011
Published in print edition November, 2011